



HAL
open science

Nanopowder synthesis of the SOFC cathode material $\text{Nd}_2\text{NiO}_{4+\delta}$ by ultrasonic spray pyrolysis

David Mesguich, Jean-Marc. Bassat, Cyril Aymonier, Elisabeth Djurado

► **To cite this version:**

David Mesguich, Jean-Marc. Bassat, Cyril Aymonier, Elisabeth Djurado. Nanopowder synthesis of the SOFC cathode material $\text{Nd}_2\text{NiO}_{4+\delta}$ by ultrasonic spray pyrolysis. *Solid State Ionics*, 2010, 181 (21-22), pp.1015-1023. 10.1016/j.ssi.2010.05.041 . hal-00547537

HAL Id: hal-00547537

<https://hal.science/hal-00547537>

Submitted on 16 Dec 2010

HAL is a multi-disciplinary open access archive for the deposit and dissemination of scientific research documents, whether they are published or not. The documents may come from teaching and research institutions in France or abroad, or from public or private research centers.

L'archive ouverte pluridisciplinaire **HAL**, est destinée au dépôt et à la diffusion de documents scientifiques de niveau recherche, publiés ou non, émanant des établissements d'enseignement et de recherche français ou étrangers, des laboratoires publics ou privés.

Nanopowder synthesis of the SOFC cathode material

$\text{Nd}_2\text{NiO}_{4+\delta}$ by Ultrasonic Spray Pyrolysis

*David Mesguich^a, Jean-Marc Bassat^a, Cyril Aymonier^a and Elisabeth Djurado^{*b}*

^a CNRS, Université de Bordeaux, ICMCB, 87 avenue du Dr. A. Schweitzer, Pessac, F-33608, France.

Fax : +33 (0)5 56 40 00 27 61 ; Tel : +33 (0)5 56 40 00 27 53 ; E-mail: mesguich@icmcb-bordeaux.cnrs.fr

^b LEPMI-Grenoble INP, UJF, CNRS, Domaine Universitaire, 1130 rue de la piscine

BP 75, 38402 Saint Martin d'Hères Cedex, France

Fax : +33 (0)4 76 82 67 77; Tel : +33 (0)4 76 82 66 84; E-mail: elisabeth.djurado@lepmi.inpg.fr

Nanostructured particles of $\text{Nd}_2\text{NiO}_{4+\delta}$ with controlled crystallinity, size and morphology have been prepared via ultrasonic spray pyrolysis. This is, to the best of our knowledge, the first time this technique has been used to synthesize this material which is of high interest for intermediate temperature solid oxide fuel cells (IT-SOFC). Spherical, submicron particles composed of nanosized crystallites of $\text{Nd}_2\text{NiO}_{4+\delta}$ are obtained at 1100 °C for reaction times typically less than 10 seconds. Amorphous to highly crystalline powders are produced depending on the reaction temperature (700-1100 °C). The particle size can be adjusted in a broad range from 50 nm to 1 μm by adjusting the initial precursor concentration and ultrasonic frequency while the powder morphology is controlled by the nature of the precursors and their concentration.

Keywords: Solid oxide fuel cell, mixed ionic and electronic conductor, nickelate, nanoparticle, Ultrasonic spray pyrolysis (USP).

I. INTRODUCTION

Solid oxide fuel cells (SOFC) convert the chemical energy of a fuel into electricity and heat while providing a promising way to produce energy in an environment-friendly way. Most efforts are turned towards reducing their operating temperature from 1000 °C to 700 °C and now 600 °C, decreasing chemical and mechanical constraints on all the components and allowing the use of cheaper materials such as stainless steel interconnects¹. However conductivity processes involved in both electrodes and the electrolyte are essentially temperature-driven and there is a strong need to improve their performances at intermediate temperatures, in particular on the cathode side. The cathode material $\text{Nd}_2\text{NiO}_{4+\delta}$, which can be referred to as a mixed ionic and electronic conductor (MIEC), exhibits a reasonable electronic conductivity associated with an important ionic conductivity due to its structural oxygen over-stoichiometry²⁻⁵. Its electrocatalytic properties (surface exchange coefficient, k), oxygen transport properties (oxygen diffusion coefficient, D^*)^{6, 7} and electrochemical properties have been previously reported⁸. This material already shows very interesting properties at 600 °C while the interfacial resistance between the cathode and the electrolyte has been identified as the limiting step in the process of oxygen reduction⁹. In order to overcome this problem, the authors have explored an original route to synthesize cathode nanostructured powders which could lead to interesting microstructures.

This work is dedicated to the synthesis of $\text{Nd}_2\text{NiO}_{4+\delta}$ nanostructured particles by ultrasonic spray pyrolysis (USP). With USP, ultrasound is used to produce precursor solution droplets dispersed in a carrier gas. The powder is generated with spherical morphology after evaporation, drying and decomposition of the precursors during the heating step. This method allows the synthesis of complex oxides submicron powders at relatively low temperatures. In this process, the powders are calcined in a very short time: 1–10 s, the oxides produced are composed of nanocrystalline particles, eliminating the need for post-treatments. The control of the primary particle diameter using the process parameters is

one of the most important advantages of this synthesis method since it allows fine control of the particle size and morphology. Indeed, the reactions responsible for product formation are confined within the individual micrometer-sized droplets which act as individual chemical reactors. If the aerosol droplet number concentration is high enough, the droplets may collide due to Brownian motion, inertia effects, electrostatic attraction and their combinations¹⁰ and form agglomerates. The agglomerates may remain as agglomerate particles containing primary crystallites. The four main operating parameters controlling properties of the final powders are the concentration of the precursor solution, the ultrasonic frequency, the furnace temperature and the carrier gas flow rate. Simply changing one of these four parameters will change the size of the particle and consequently the primary particle diameter and the morphology. As reported earlier¹¹, the control of USP parameters has allowed tuning zirconia powder properties, especially the primary particle size, agglomerate particle size and morphology.

In addition, all spherical aerosol droplets are separately pyrolysed in a short time to form discrete solid particles, providing a moderate size distribution. Ultrasonic spray pyrolysis has been applied to material synthesis for more than 20 years¹² and is based on a patent from 1972¹³. It has been successfully applied to the synthesis of various oxides such as zirconia^{11, 14}, ceria¹⁵ or NiO-ceria composite¹⁶. This is a fast, high yielding method associated with moderate cost and very short reaction times suitable to synthesize highly crystalline oxides nanoparticles with tuneable size and morphology as demonstrated in previous studies^{11,12, 14-17}. Moreover the purity of the products is high and the composition of powders is easy to control. As-synthesized powders are generally composed of crystalline spherical particles.

The first part of this paper is devoted to the selection of the spray-pyrolysis experimental conditions, and then the influence of the operating parameters on the properties of the cathode powders is discussed.

II. EXPERIMENTAL SECTION

The ultrasonic spray pyrolysis method relies on the pyrolysis of an aerosol generated by ultrasonic pulverisation. This process can be described in four steps:

1 Ultrasonic pulverisation of a precursor solution generates an aerosol of droplets.

2 Aerosol droplets are carried via a gas flow through the furnace.

3 High temperature in the furnace induces evaporation of the solvent and precipitation of the solubilised species which are dried and then decomposed into metal oxides.

4 Dry powders are collected using an electrostatic filter.

Two different types of precursors were used in order to change the chemistry and evaluate their influence on the powder properties. Neodymium oxide (Nd_2O_3 , 99.9%, Alfa Aesar) and nickel nitrate hexahydrate ($\text{Ni}(\text{NO}_3)_2 \cdot 6\text{H}_2\text{O}$, Sigma-Aldrich) were used as starting powders. Neodymium oxide was first dissolved into a slight excess of nitric acid (HNO_3 , 68 w% in water, Prolabo). Then the neodymium nitrate solution was diluted in distilled water to reach the desired concentration. Nickel nitrate was easily dissolved into distilled water, then both nitrates solution were mixed together in a stoichiometric amount ($\text{Nd}:\text{Ni} = 2:1$).

Neodymium acetate ($\text{Nd}(\text{CH}_3\text{COO})_3$, 99.9%, Sigma-Aldrich) and nickel acetate ($\text{Ni}(\text{CH}_3\text{COO})_2$, 99+%, Alfa Aesar) have also been used. These precursors are easily dissolved in water in stoichiometric amounts and mixed together at room temperature. The final solution was introduced into the high-frequency ultrasonic mist generator at room temperature.

Two different piezoelectric ceramic transducers have been used, characterized by 2.5 and 1.7 MHz frequencies. Two synthetic air (80% N_2 , 20% O_2) flow rates of 3 and 6 $\text{L}\cdot\text{min}^{-1}$ were selected to carry the formed aerosol through the 3-zones high temperature furnace. Temperature in the last two zones was fixed at 700 °C, 900 °C or 1100 °C, the first zone always being set 50 °C lower to avoid too fast evaporation of the solvent and heterogeneous precipitation of the solute (for details on the experimental setup please refer to ¹⁸).

Crystallographic structure of the powders was characterized by X-ray powder diffraction (XRD, PANalytical X'Pert MPD diffractometer in θ - θ configuration with a $\text{Cu K}\alpha$ radiation ($\lambda=1.5418 \text{ \AA}$)) over the 2θ range 5-80 ° in a $0.036^\circ\cdot\text{s}^{-1}$ continuous scan mode at room temperature. Morphology of the particles was studied by high resolution scanning electron microscopy (HR-SEM, JEOL 6700) under 5.0

kV accelerated voltage and transmission electron microscopy (MET JEOL 2000). The particle size was evaluated from the SEM micrographs by manual counting over 500 particles using Image Tool software. Chemical purity was determined by elementary analyses of the powders using inductively coupled plasma-optical emission spectrometry (ICP-OES, Varian 720-ES) and CHNS microanalyser (ThermoFisher FlashEA 1112). Thermal analyses were performed with a Netzsch STA 409 C/CD apparatus under an air (or Ar/H₂) flow of 100 ml.min⁻¹ (heating rate 4°C.min⁻¹ from room temperature up to 1000 °C).

III. RESULTS AND DISCUSSION

Nd₂NiO_{4+δ} is a mixed ionic and electronic conductor exhibiting oxygen overstoichiometry inducing high ionic conductivity, however it is unsure whether high crystallinity is required in order to optimize its transport properties or not. Since the aim of this work is to obtain highly controlled nanoparticles of Nd₂NiO_{4+δ}, research efforts were focused on studying the influence of the spray-pyrolysis experimental parameters (reaction temperature, precursor nature and precursor concentration, carrier gas flow rate and atomizing frequency) in order to tune the physical and chemical properties of the powder such as the crystallinity, particle size and morphology. Experimental conditions of the different experiments are presented in Table 1. All samples are referred to as NdN x for x experiment.

1. Control of the powder crystallinity, crystallite size and chemical composition. Reaction temperature is the key parameter which controls the crystalline nature of the powders synthesized as illustrated in Figure 1. At moderate temperatures (700 °C), the powders are mainly amorphous as confirmed by XRD showing no diffraction peaks. Raising the reaction temperature up to 900 °C leads to crystalline Nd₂NiO_{4+δ} powders with an average crystallite size of approximately 10-20 nm (estimated using the Debye-Scherrer's formula on the most intense reflection, (113)). Neodymium oxide, Nd₂O₃, is also present. It is worth noticing that in spite of the very short residence time (less than 10 seconds), the

refractory oxide begins to crystallize at 900 °C which is a moderate crystallisation temperature in comparison with other syntheses such as gel routes and solid state reaction (1000-1200 °C range^{2-4, 6, 7}). Highly crystalline powders (average crystallite size 30-40 nm) are obtained when the reaction temperature is 1100 °C with the possible presence of a unique impurity, Nd₂O₃, detected in minority in comparison with powders synthesized at 900 °C. XRD comparison shown in Figure 2 clearly demonstrates different steps in the powder calcinations when the synthesis temperature is 700 °C. Heat treatment at the pyrolysis temperature (i.e. 6 h at 700 °C) induces crystallisation of the powder indicating that the very short reaction time inhibits crystallisation during the synthesis at moderate temperature. The most intense peaks are very wide and their position matches well with the theoretical position of the Nd₂NiO_{4+δ} diffraction peaks whereas sharper peaks are attributed to Nd₂O₃ both in its hexagonal and cubic lattice. Heating up to 800 °C promotes crystallization of hexagonal Nd₂O₃ over the cubic phase, apart from this the XRD pattern remains essentially similar. The most interesting phenomenon occurs between 800 °C and 900 °C: Nd₂NiO_{4+δ} phase quickly crystallises and Nd₂O₃ impurity is removed even when the calcination step is reduced to 1 hour. Ni nitrate is decomposed in NiO around 300 °C¹⁹ whereas the formation of Nd₂O₃ from Nd nitrate thermal decomposition is reported around 550-800 °C^{20, 21}. Nevertheless, Nd₂O₃ crystallization is observed after annealing the powders at 700 °C indicating the effective decomposition of the neodymium nitrate at this temperature. As a consequence, besides the precursors thermal decomposition, the thermodynamics and kinetics governing the formation of the mixed oxide Nd₂NiO_{4+δ} should be taken into account to explain the annealing behavior of the powders. The authors assume that the lowering of the crystallization temperature of Nd₂NiO_{4+δ} is directly enabled by the characteristics of the powders synthesized by USP; the combination of the extremely small crystallite size, small particle size and high homogeneity of the powders greatly enhancing the powder reactivity. For instance, after such annealing (900 °C, 1 h), the crystallite size is 42 nm (for a synthesis temperature of 700 °C, precursor solution concentration 5.10⁻³ M and atomising frequency 1.7 Hz). Further annealing only slightly increases the grain size up to 47 nm and 52 nm respectively for calcinations of 6 h at 1000 °C and 36 h at 1100 °C. The spray pyrolysis

synthesis at 700 °C leads to a highly reactive amorphous Nd-Ni "precursor" which quickly converts into $\text{Nd}_2\text{NiO}_{4+\delta}$ phase after calcinations at 900 °C for 1 h. Crystallite growth is limited (in this case around 50 nm) even after lengthy heat treatments. This has been reported in previous USP experiments²² and may be due to two reasons: (i) nanocrystallites are agglomerated in a crystallized envelope; (ii) the high purity of the materials.

A subsequent heat treatment at 900 °C in air (typically 1 to 6 h) is sufficient to either induce the crystallisation of $\text{Nd}_2\text{NiO}_{4+\delta}$ for powders synthesized at 700 °C or promote further crystallisation of the mixed oxide and remove the Nd_2O_3 impurity for powders synthesized at 900 or 1100 °C. After such heat treatment at 900 °C the crystallite size is approximately 35-40 nm, which means crystallite growth is limited to about 10 % for samples synthesized at 1100 °C whereas crystallite size is at least doubled for samples synthesized at 900 °C. Further annealing steps up to 1100 °C for 36 h cause a slight increase in crystallite size up to 45-52 nm independent of the initial reaction temperature. The limited crystallite growth in samples synthesized at 1100 °C, even after 36 h of calcinations, proves that these powders are already highly crystalline before any heat treatment. The evolution of the $\text{Nd}_2\text{NiO}_{4+\delta}$ crystallite size as a function of the pyrolysis temperature and heat treatments is presented in Table 2. This table shows that the crystallite size of fresh powders primarily depends on the pyrolysis temperature. At 700 °C powders are amorphous whereas $\text{Nd}_2\text{NiO}_{4+\delta}$ is crystallized at 900 °C and 1100 °C and the crystallite size is doubled for the higher pyrolysis temperature (15 ± 2 nm and 35 ± 3 nm respectively). However, these differences quickly disappear after annealing under air; for instance the crystallite size is comprised between 38 ± 2 and 42 ± 2 nm after 6 h of heat treatment at 900 °C and between 48 ± 3 and 52 ± 2 after 36 h of heat treatment at 1100 °C no matter the pyrolysis temperature. After annealing at 900 °C (and above) the powders share similar crystallite sizes.

The influence of the residence time on the powder crystallinity has been studied as well. Indeed, XRD patterns for samples synthesized with 8 s residence time (gas flow rate of $6 \text{ L}\cdot\text{min}^{-1}$) and 16 s residence time (gas flow rate of $3 \text{ L}\cdot\text{min}^{-1}$) are very similar when the reaction temperature is 700 °C. For higher temperatures (i.e. 1100 °C), further reaction time favours $\text{Nd}_2\text{NiO}_{4+\delta}$ over Nd_2O_3 crystallization.

However, in this time range, influence of the reaction time on the crystallite growth is absolutely negligible. As exposed above, the crystallite growth is very limited so further reaction time allows a more complete reaction towards the formation of the mixed oxide without affecting its crystallite size.

Chemical composition of the powders has been evaluated by elemental analyses and thermal analyses. Inductive Coupled plasma analysis has been performed to check the Nd:Ni molar ratio which is consistently between 1.95 and 2.00, the cation stoichiometry of the powders matching the stoichiometry of the starting solution (except for the experiments using acetates where a high deficiency in neodymium was found probably due to different kinetics between the neodymium and the nickel precursor in the experimental conditions). CHNS elemental analysis allows quantifying the organic residue in the powders. A low nitrogen content of the powders was found from 0.5 to 1.0 wt % from nitrate precursors. This could be due to low concentration and high reaction temperature which favour lower nitrogen content due to better decomposition of the nitrates precursors. The hydrogen content of about 0.5 wt % was measured mostly due to the low water condensation in the electrostatic filter in the end of the experiment. For example, the composition of NdN 3 (pyrolysis temperature of 1100 °C) in molar percentage is Nd: 19,2, Ni: 9,8, O: 45,8, N: 2,5, H: 22,7, (or given in weight percentage Nd: 66,9, Ni: 13,9, O: 17,7, N:0,9, H: 0,6). Thermogravimetric analysis was in good agreement with elemental analyses; the total mass loss at 1000 °C was 8 ± 2 wt % for experiments with low pyrolysis temperature (700 °C) which corresponds to loss of water and residual nitrogen oxides and less than 4 wt% for experiments with high (1100 °C) pyrolysis temperature.

The ability to stabilize excess oxygen in the lattice is the structural feature enabling the ionic conductivity of $\text{Nd}_2\text{NiO}_{4+\delta}$ thus it is much related to its application as a mixed ionic and electronic conductor for SOFCs. Oxygen content of this type of oxides can vary depending on the synthesis process (particularly on the process temperature and atmosphere) as well as physico-chemical properties of the powders such as the cation stoichiometry and the crystallite size as shown in previous studies on the oxygen content of such nickelates²³. Iodometric titration experiments have been performed to quantify the Ni^{3+} content corresponding to the oxygen overstoichiometry (noted δ) of the $\text{Nd}_2\text{NiO}_{4+\delta}$

powders produced by USP. Such experiments have been performed on powders NdN 6 and NdN 10 pyrolysed at 1100 °C with corresponding atomisation frequencies of 1.7 MHz and 2.5 MHz respectively. The measured δ values for the as-obtained powders (without heat treatment) ranging in 0.14-0.15 are slightly lower than reported values for $\text{Nd}_2\text{NiO}_{4+\delta}$ around 0.19⁶-0.22². Indeed these values are quite high considering the very short pyrolysis step of 8 s; this underlines the high reactivity of the powders which can accommodate a reasonable amount of overstoichiometric oxygen in a very short time. Heat treatment at 900 °C under air during 10 h has been applied to the powders in order to reach the equilibrium value of δ ; this treatment effectively enhances the value of δ to 0.22-0.24, comparable to the data available in the literature.

2. Control of the particle size, 2.a. Calculation of the theoretical particle size. Previous studies have shown a strong correlation between the particle size and the precursor concentration and ultrasonic frequency^{11, 14, 15, 24}. This theoretical relation is reported as Lang's equation (Equation 1) linking the mean diameter of the aerosol droplets (D in μm) to the surface tension of the atomised solution (σ in $\text{N}\cdot\text{m}^{-1}$), the density of the solution (ρ in $\text{g}\cdot\text{cm}^{-3}$) and the ultrasonic frequency of the piezoelectric ceramic transducers (f in Hz)²⁵.

$$D = 0.34 \times 10^6 \left(\frac{8\Pi\sigma}{\rho f^2} \right)^{1/3} \quad (1)$$

This equation shows that the droplet size depends on the ultrasonic frequency to the power $-2/3$. Assuming that low concentration precursor solutions have similar σ and ρ values as pure water ($\sigma=72.9\cdot 10^{-3} \text{ Nm}^{-1}$, $\rho=1 \text{ g}\cdot\text{cm}^{-3}$ at 20 °C, 1 atm), the droplet size is expected to vary between 2.70 μm ($f=1.7 \text{ MHz}$) and 2.08 μm ($f=2.5 \text{ MHz}$). The theoretical mean particle diameter is directly related to the aerosol droplet size as shown in Equation 2 linking the theoretical mean diameter of fully dense particles (d_0 in nm) to the final oxide (*i.e.* $\text{Nd}_2\text{NiO}_{4+\delta}$) concentration in respect to the concentration of the precursor solution used (C in $\text{mol}\cdot\text{L}^{-1}$), the molar mass of the oxide (M in $\text{g}\cdot\text{mol}^{-1}$), the aerosol droplet

mean diameter (D in μm as calculated in Eq. 1) and the theoretical density of the final oxide (ρ_{ox} in g.cm^{-3}).

$$d_0 = 10^3 \left(\frac{10^{-3} \times C.M.D^3}{\rho_{\text{ox}}} \right)^{1/3} \quad (2)$$

From these two equations one can infer that the theoretical particle size depends on the concentration to the power 1/3 and on the ultrasonic frequency to the power -2/3. Simple calculation shows that in the experiments presented here the theoretical particle size d_0 varies from 63 nm ($C=5.10^{-4}$ M, $f=2.5$ MHz) to 378 nm ($C=5.10^{-2}$ M, $f=1.7$ MHz). One should note that this calculation does not take into account the effect of the carrier gas flow rate (controlling residence time) or the effect of the pyrolysis temperature.

A comparison between theoretical and experimental particle sizes is shown in Table 1. The experimental mean particle size ($d_{0.5}$, 50% of the particles are below this size) is always higher than the theoretical one, especially when the concentration and the temperature are high and the flow rate is low. As underlined earlier, the theoretical particle size estimated by Lang's equation is just an estimation taking into account only the physico-chemical characterisations of the precursor solution but is not dependent of the technical spray-pyrolysis parameters such as the temperature and the flow-rate. Moreover, the average particle size is always 15-20% larger than the mean particle size, the former being shifted towards high values by scarce very large particles.

2.b. Influence of the precursor concentration. Varying the concentration of the nitrates precursor solution proves to be an effective way to control the particle size as evidenced in SEM observations (Figure 3, note the difference in the scale bars). With increasing concentration from 5.10^{-4} M to 5.10^{-3} M and 5.10^{-2} M while keeping constant pyrolysis temperature at 700°C , air flow rate at 6 L.min^{-1} and atomising frequency at 1.7 MHz, the mean particle size increases from 108 nm to 190 nm and 542 nm respectively. Multiplying the concentration by a factor of 100 leads to a dramatic increase in size by roughly a factor of 5 which is in agreement with the theoretical dependence of the size on the concentration to the power 1/3 as predicted by Lang's equation.

2.c. *Influence of the atomizing frequency.* Figure 4 demonstrates the influence of the ultrasonic frequency from 1.7 MHz to 2.5 MHz on the particle size and size distribution (keeping constant the concentration of the nitrates precursor solution at 5.10^{-4} M, pyrolysis temperature at 700°C , air flow rate at $6 \text{ L}\cdot\text{min}^{-1}$). In these given conditions, experimental mean particle size is estimated to be respectively 67 nm and 108 nm for a frequency of 2.5 and 1.7 MHz. As predicted, high atomizing frequency slightly reduces the particle size but also significantly decreases the amount of large particles thus narrowing the size distribution as shown in Figures 4 and 5. As a consequence, the experimental and theoretical particle sizes are in better agreement for higher frequencies. The ultrasonic frequency parameter has more influence on the particle size distribution when the concentration of the precursor solution is low as shown in Figure 5.

2.d. *Influence of the residence time.* The influence of the residence time over the particle size has also been studied varying the flow rate from $3 \text{ L}\cdot\text{min}^{-1}$ to $6 \text{ L}\cdot\text{min}^{-1}$ keeping constant the concentration of the nitrates precursor solution at 5.10^{-3} M, pyrolysis temperature at 700°C and atomising frequency at 1.7 MHz. Reducing the flow rate from $6 \text{ L}\cdot\text{min}^{-1}$ to $3 \text{ L}\cdot\text{min}^{-1}$ extends the residence time from 8 to 16 seconds which is expected to increase both the crystallite and particle size. Indeed, slower flow rates increase the residence time for each droplet within the furnace enhancing diffusion phenomena. Simultaneously, a smaller flow rate should lead to a decrease of the droplet number density. Consequently, collisions and droplet coalescence should be reduced providing a reduction in particle size. The flow rate parameter is of less importance on the particle size due to these both competitive phenomena. Indeed, this effect was observed in our experimental data (table 1). The mean particle size for experiments NdN 5 (flow rate of $6 \text{ L}\cdot\text{min}^{-1}$) and NdN 13 (flow rate of $3 \text{ L}\cdot\text{min}^{-1}$) are indeed very similar, 190 and 187 nm respectively. This result suggests that the particle formation and growth could be very fast and then reach a plateau for given conditions (*i.e.* temperature, concentration, pulverisation frequency). The droplet size of the aerosol should not be influenced by the carrier gas flow rate, once the solvent has been evaporated out of the droplet and all its inorganic content has precipitated, the inorganic particle freshly formed would have a define size and its main growth mechanism would be the

consequence of an aggregation of other inorganic particles. The similar size in both experiments would suggest that the growth is completed after 8 seconds; consequently further reaction time does not induce any further growth. One should note that 8 seconds is the lowest residence time that was tried for these experiments.

2.e. Influence of the reaction temperature. Reactions have been carried out at various temperatures of 700 °C, 900 °C and 1100 °C while keeping constant the concentration of the nitrates precursor solution at 5.10^{-3} M, atomising frequency at 1.7 MHz. and flow rate at 6 L.min⁻¹. Difference in reaction temperatures causes little variations in the particle size. Comparison of the particle size confirms a slight increase in size from 190 to 224 nm when the temperature rises from 700 °C to 1100 °C. From the XRD patterns (Figure 1), a narrowing of XRD peaks corresponding to Nd₂NiO_{4+δ} crystallite growth was observed. The crystallite size increases from 13 nm to 34 nm when the temperature rises from 900 °C to 1100 °C. Indeed, as previously reported^{11, 14}, the pyrolysis temperature is the main factor which controls the crystallite growth due to diffusion phenomena. However, as already discussed above, a limited crystallite growth in the particles is observed, in agreement with previous works²².

It can be noted that no matter the experimental conditions, the particle size distribution is always quite broad and asymmetric with a larger proportion of particles greater than the mean particle size. This uneven distribution, which is quite reduced in the experiments presented, is typical of the spray pyrolysis process. This size distribution could best be explained as a random coagulation of mist particles, the initial collision of various droplets would result in a large size distribution of droplets, then in a large size distribution of the particles after pyrolysis. Typically, the difference between the smaller and the larger particles is one order of magnitude. Decreasing the precursor concentration, as well as raising the ultrasonic frequency help reducing the particle size distribution; this effect is much related to the decrease in aerosol droplets (and consequently particle size) already mentioned for these two parameters. As the aerosol droplets produced are smaller, their tendency to collide is lowered, eventually leading to a more uniform droplet size therefore to the narrowing of the particle size distribution.

Moreover, whereas Lang's equations implicitly refer to a unique reaction mechanism (one-particle-per-drop), in the ultrasonic spray pyrolysis process, particles should be formed after different steps during the pyrolysis by the evaporation of the solvent followed by the precipitation of the solute, then the drying step and ultimately the conversion to oxide. The resulting particles are typically consisted in aggregates of primary grains that are representative of crystallites.

Using spray pyrolysis $\text{Nd}_2\text{NiO}_{4+\delta}$ particles in a broad size range from 50 nm up to 1 μm have successfully been produced. The particle size and size distribution were monitored via careful choice of the experimental parameters, essentially the precursor solution concentration and the atomizing frequency as can be expected from theoretical equations 1 and 2. The same parameters, especially the ultrasonic frequency affect the particle size distribution as well. These submicron powders should lead to significant electrical changes when applied as cathodes materials coated onto SOFC electrolytes.

3. Control of the morphology. The obtained powders are generally composed of spherical and relatively smooth particles as confirmed by SEM in Figures 3 and 4 for powders prepared varying the concentration of the solution of precursors and/or the frequency of the atomiser. Influence of the temperature on the particle morphology is more important when the precursor solution concentration is high. At low concentrations ($5 \cdot 10^{-4}$ M), particles are always spherical and smooth while at high concentrations when the synthesis temperature is 700 °C particles exhibit an irregular surface with lots of bumps and for 1100 °C particles are much more distorted and exhibit some porosity. The initial solution saturation (ratio C_o/C_s between the precursor concentration in the starting solution C_o and the precursor saturation concentration C_s) has proved to be a crucial factor for the control of the particle morphology^{12, 15, 24, 26}. In order to obtain solid spherical particles C_o/C_s should be equal to or less than 0.01. For experiments conducted from nitrates, this ratio is always under the aforementioned limit except when the concentration is $5 \cdot 10^{-2}$ M (Figure 3c), C_o/C_s is then 0.006 for the nickel nitrate and 0.03 for the neodymium nitrate. It is clear from the SEM (Figure 6) and TEM micrographs (Figure 7) that at

low concentrations (*i.e.* 5.10^{-4} M), the particles are spherical and perfectly smooth but the shape becomes more irregular and the surface rougher when the concentration is increased.

Finally, the nature of the precursors is also determining. Particle morphology is significantly affected when the precursors were changed from nitrates to acetates. As shown in SEM view (Figure 8), a majority of hollow and twisted particles are observed from acetates precursors. This final morphological difference in between both powders can be explained by a drastic difference in solubility between acetate and nitrate precursors as shown by the solubility values (in water at 20 °C) provided by the chemical suppliers: neodymium acetate 260g/l, nickel acetate 270 g/l, neodymium nitrate 1529 g/l, nickel nitrate 2380 g/l. Indeed the acetates are less soluble in water than the corresponding nitrates by approximately one order of magnitude. In sample prepared with a 10^{-2} M acetate concentration (at 700 °C and 1.7 MHz frequency), the C_o/C_s ratio is 0.026 for the neodymium acetate and 0.01 for the nickel acetate. To understand why the initial solution saturation is so important during the evaporation step of the pyrolysis process, we have to focus on the solute concentration. The concentration of the dissolved salt depends on the initial concentration and the droplet size, thus increases with droplet shrinkage, eventually leading to precipitation of the inorganic precursor inside the droplet. However, the solute concentration is not uniform throughout the evaporation period, because the evaporation rate at the droplet surface is faster than the rate of the solute diffusion, resulting in higher concentration at the droplet surface than its center¹². When precipitation occurs, the evaporation rate and mass transfer are greatly reduced. Surface precipitation becomes significant for high concentrations, especially above an initial solution saturation value of 0.01^{15, 24}. Due to the low solubility of the solute, precipitation occurs much faster in the early stages of the process forming a shell on the drop surface; a large amount of water is thus trapped inside the drop. The water is evaporated as the temperature increases leaving a void inside the particle eventually causing greater plastic deformation and shrinkage in the latter stages. The resulting particles obtained are faceted with irregular shapes of polyhedral (Figure 8).

For the same reason, when the nitrate concentration is high, the bigger particles have irregular shapes, rough surfaces and appear to be hollow (Figure 9). In fact, SEM observations show that the amount of

hollow particles increases when the concentration is high. This suggests that precipitation occurs on the surface instead of the entire volume of the aerosol droplet because of the high initial solution saturation. In a given sample, the hollow particles are among the largest ones since the solute concentration gradient (eventually leading to surface precipitation and hollow particles) is increased with the droplet radius. Moreover higher concentrations increase density of matter inside the droplet and therefore lead to an increase of internal stresses during particle formation which can explain this surface phenomenon^{11, 14}. Previous authors¹⁵ also suggest that releasing gas from the larger particles through small pores or cracks would be more difficult than releasing gas from the smaller particles; therefore the gas would remain in the large particles as voids¹⁶.

The atomizing frequency has a slight influence on particle morphology. Namely, the rate of evaporation of droplets, heat transport phenomenon and diffusion processes in the droplets all depend on the droplet size. When ultrasounds are used at lower frequencies, from 1.7 MHz with comparison to 2.5 MHz, larger droplet sizes are estimated as reported above in paragraph 2 (2.70 μm and 2.08 μm , respectively) and according to equation 1. During the evaporation step, the pressure development inside the larger drying droplets/particles should be reduced yielding to a slower evaporating rate. This causes a certain roughness on the particle surface, increases the probability of superficial crystallisation on the larger particles while high frequencies lead to smooth particle surfaces.

The particle morphology is effectively controlled by the concentration of the precursor solution and the nature of the precursors based on solubility while surface roughness is strongly influenced by the atomizing frequency.

IV. CONCLUSIONS

The ultrasonic spray pyrolysis method has been successfully applied to the synthesis of $\text{Nd}_2\text{NiO}_{4+\delta}$ nano-sized powders for the first time. This study demonstrates the suitability of the spray pyrolysis method to obtain cathode nanopowders. The crystallinity, size and morphology of the particles were

easily tuned varying the experimental parameters such as the precursor concentration, the atomizing frequency and the reaction temperature. The powder crystallinity can be varied from amorphous to highly crystalline by simply adjusting the reaction temperature. It is highly remarkable to obtain these crystalline mixed oxide powders after such short reaction times. Furthermore, when amorphous powders are obtained, the reactivity from just minimal heat treatment (900 °C, 1 h) is sufficient to convert these powders into highly crystalline $\text{Nd}_2\text{NiO}_{4+\delta}$, whereas other routes require longer post treatments^{6,7}.

Spherical particles were obtained in a very wide size range, from tens of nanometers up to the micron scale. Moreover the broad particle size distribution usually obtained using this process has been narrowed via optimisation of the operating parameters (low concentration and high atomizing frequency). The morphology of the particles was controlled via the nature of precursors and concentration of the precursor solutions in respect to the saturation concentration. The particles synthesized can be very smooth and regular in shape (at low concentrations) or highly distorted, bumpy and appear hollow (at high concentrations). The authors would like to emphasize that the ability given by the present method to obtain $\text{Nd}_2\text{NiO}_{4+\delta}$ nanopowders, either amorphous or highly crystalline with similar particle sizes and morphology, will allow the effect of the cathode in-situ crystallisation onto the electrolyte and its electrochemical properties to be studied. Electrochemical properties of these nanopowders applied as a cathode layer are currently being investigated by impedance spectroscopy and will soon be reported.

LIST OF REFERENCES

- 1 B.C.H. Steele, A. Heintzel, *Nature* 414 (2001) 345.
- 2 E. Boehm, J.-M. Bassat, P. Dordor, F. Mauvy, J.-C. Grenier, Ph. Stevens, *Solid State Ionics* 176 (2005) 2717.
- 3 G. Amow, S. Skinner, *J. Solid State Electrochem.* 10 (2006) 538.
- 4 C. Lalanne, G. Prosperi, J.-M. Bassat, F. Mauvy, S. Fourcade, P. Stevens, M. Zahid, S. Diethelm, J. Van herle, J.-C. Grenier, *J. Power Sources* 185 (2008) 1218.
- 5 J.-M. Bassat, P. Odier, A. Villesuzanne, C. Marin, M. Pouchard, *Solid State Ionics* 167 (2004) 341.
- 6 J. Wan, J.B. Goodenough, J.H. Zhu, *Solid State Ionics* 178 (2007) 281.
- 7 C. Lalanne, F. Mauvy, E. Siebert, M.L. Fontaine, J.M. Bassat, F. Ansart, P. Stevens, J.C. Grenier, *J. Eur. Ceram. Soc.* 27 (2007) 4195.
- 8 C. Lalanne, F. Mauvy, J. M. Bassat, J. C. Grenier, D. Pordor, M. Pouchard, in: *Proc. 6th Europ. SOFC*, M. Mogensen, Ed. (2004) ISBN 3-905592-15-0, 1351.
- 9 F. Mauvy, C. Lalanne, J.M. Bassat, J.C. Grenier, H. Zhao, P. Dordor, Ph. Stevens, *J. Eur. Ceram. Soc* 25 (2005) 2669.
- 10 G. Langer, G. Yamate, *J. Coll. Interf. Sci.*, 29 (1969) 450.
- 11 E. Djurado, E. Meunier, *J. Solid State Chem.* 141 (1998) 191.
- 12 G. L. Messing, S.-C. Zhang, G. V. Jayanthi, *J. Am. Ceram. Soc.* 76 (1993) 2707.
- 13 J. Spitz, J. Viguie, French patent 2,110,622 (1972).
- 14 M. Gaudon, E. Djurado, N.H. Menzler, *Ceramics International* 30 (2004) 2295.
- 15 K. Okuyama, I. Wuled Lenggoro, *Chemical Engineering Science* 58 (2003) 537.
- 16 C.Y. Chen, T.K. Tseng, S.C. Tsai, C.K. Lin, H.M. Lin, *Ceramics International* 34 (2008) 409.
- 17 S. Suda, S. Takahashi, M. Kawano, H. Yoshida, T. Inagaki, *Solid State Ionics* 177 (2006) 1219.
- 18 R.A. Rocha, E. Muccillo, L. Dessemond, E. Djurado, *J. Eur. Ceram. Soc.* 30 (2010) 227.
- 19 W. Brockner, C. Ehrhardt, M. Gjikaj, *Thermochim. Acta* 456 (2007) 64.
- 20 T. Bataille, N. Audebrand, A. Boultif, D. Louër, *Z. Kristallogr.* 12 (2004) 881.
- 21 W. W. Wendlandt, *Anal. Chim. Acta* 15 (1956) 435.
- 22 F. Boulc'h, E. Djurado, *Solid State Ionics* 157 (2003) 335.
- 23 M.-L. Fontaine; C. Laberty-Robert; A. Barnabé; F. Ansart; P. Tailhades, *Ceramics International* 30 (2004) 2087.
- 24 S.C. Zhang, G.L. Messing, M. Borden, *J. Am. Ceram. Soc.* 73 (1990) 61.

- 25 R.J. Lang, J. Acoust. Soc. Am. 34 (1962) 6.
- 26 G. V. Jayanthi, S. C. Zhang, G. L. Messing, Aerosol Science and Technology 19 (1993) 478.

TABLES

Table 1: Experimental conditions of the spray pyrolysis experiments with corresponding theoretical and experimental particle size.

	Temperature (°C)	Concentration of the precursor solution (10 ⁻³ mol.L ⁻¹)	Air flow rate (L.min ⁻¹)	Atomising frequency (MHz)	Theoretical particle size (nm)	Experimental particle size (nm)		
						d _{0.1}	d _{0.5}	d _{0.9}
NdN 1	1100	0.5	6	1.7	81	-	-	-
NdN 2	700					65	108	215
NdN 3	1100	5			175	160	224	450
NdN 4	900					-	-	-
NdN 5	700				105	190	335	
NdN 6	1100				50	378	250	474
NdN 7	700	310		542			1250	
NdN 8	1100	0.5		2.5	63	-	-	-
NdN 9	700					44	67	96
NdN 10	1100	50			291	270	423	830
NdN 11	700		-			-	-	
NdN 12	1100	5	3	1.7	175	-	-	-
NdN 13	700					80	187	340
NdN 14 *	1100	10	6	1.7	221	140	206	320
NdN 15 *	700					-	-	-

* indicates experiments using acetate precursors instead of nitrates

Table 2: Evolution of $\text{Nd}_2\text{NiO}_{4+\delta}$ crystallite size as a function of the pyrolysis temperature and heat treatment conditions.

Pyrolysis temperature (°C)	Heat treatment temperature and duration (°C / h)	$\text{Nd}_2\text{NiO}_{4+\delta}$ crystallite size evaluated from Debye-Scherrer formula (nm)
700	-	(amorphous)
	900 / 6	42±2
	1000 / 6	47±1
	1100 / 6	47±1
	1100 / 36	52±2
900	-	15±2
	900 / 6	38±2
	1000 / 6	46±2
	1100 / 36	49±2
1100	-	35±3
	900 / 6	38±2
	1100 / 36	48±3

FIGURES

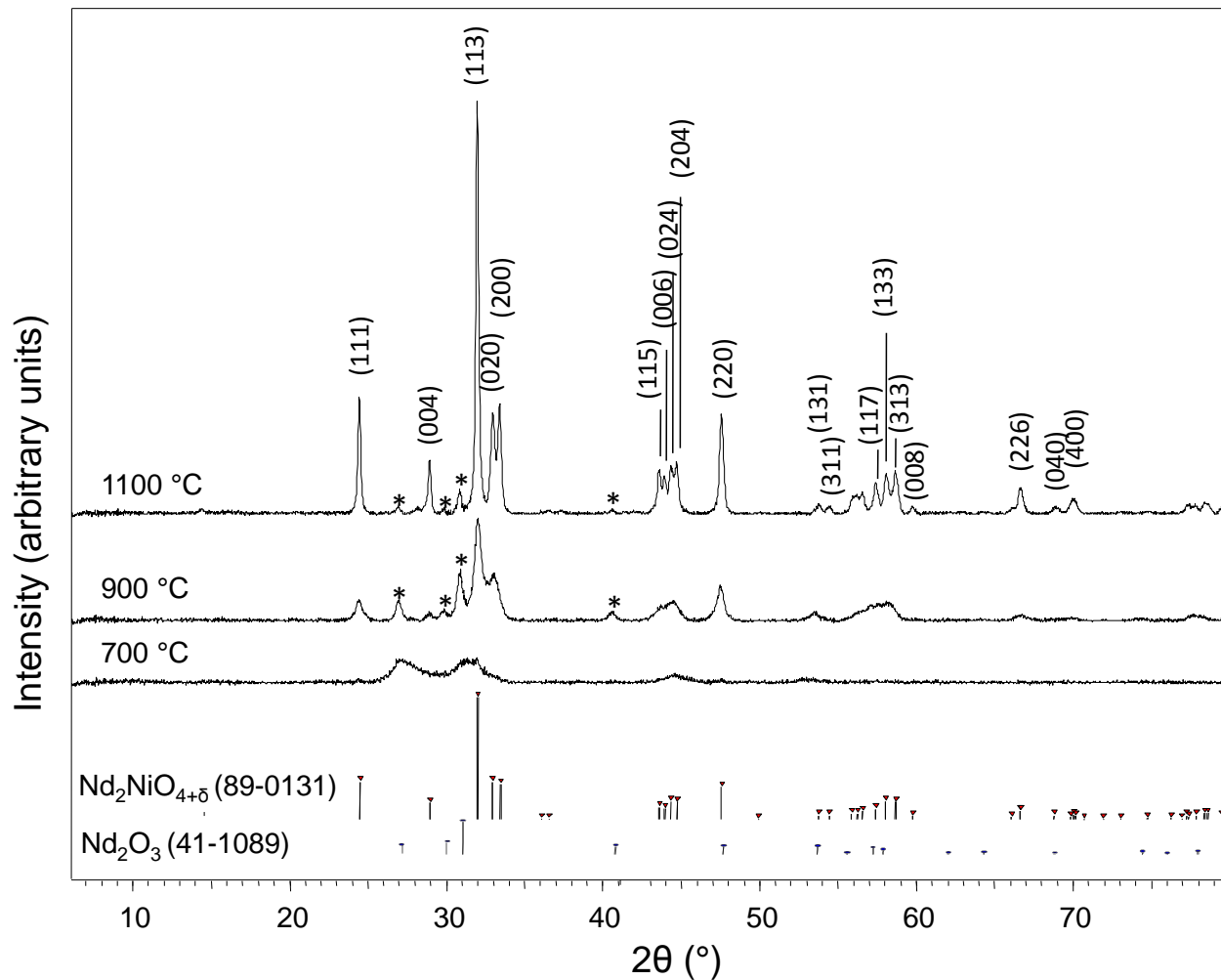


Figure 1: XRD patterns of samples NdN 3, NdN 4 and NdN 5 synthesized at different temperatures ($\text{Nd}_2\text{NiO}_{4+\delta}$ diffraction planes are indexed, * corresponds to the impurity Nd_2O_3 , references $\text{Nd}_2\text{NiO}_{4+\delta}$ (JCPDS 89-0131) and Nd_2O_3 (JCPDS 41-1089) are inserted).

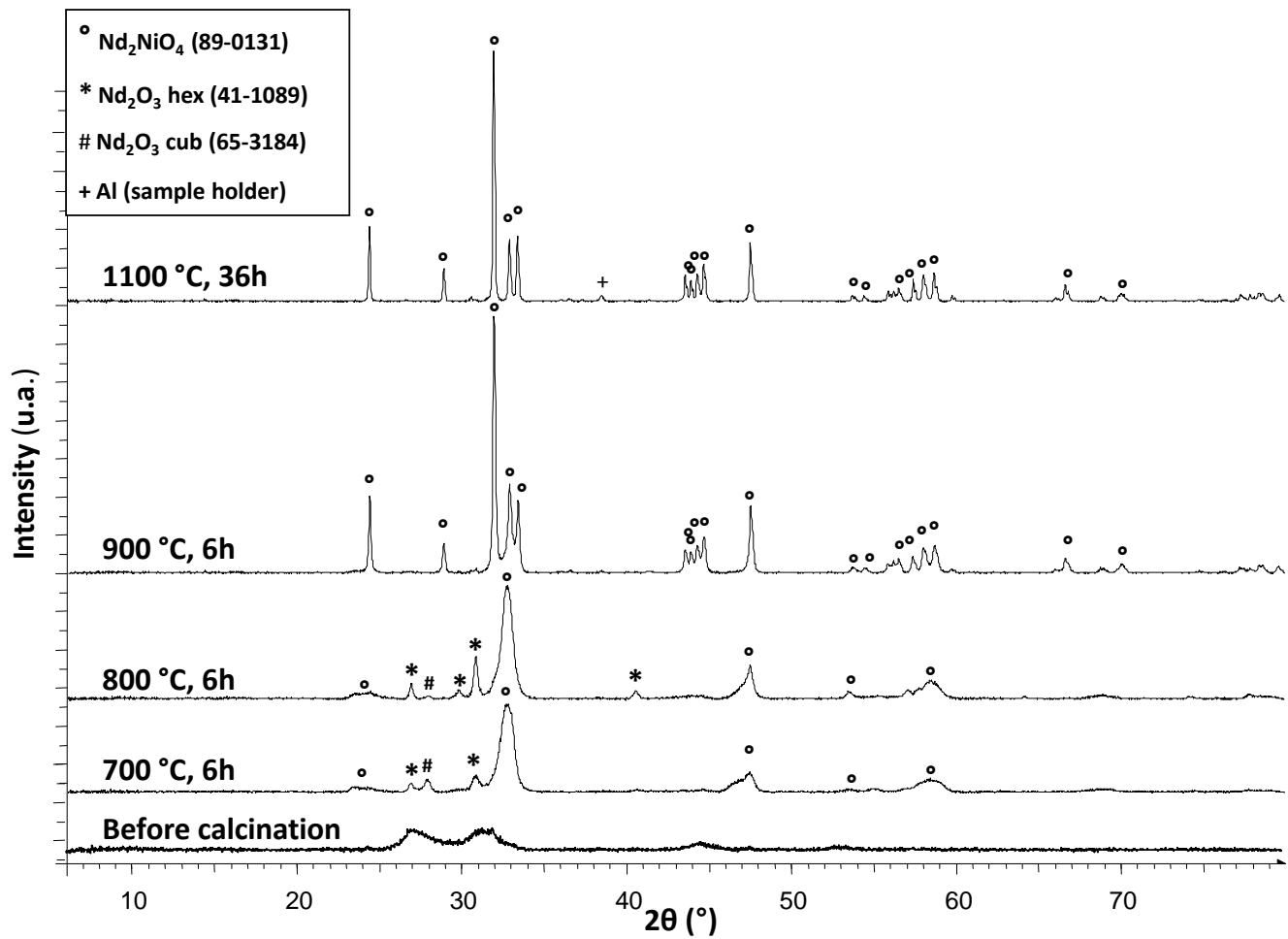


Figure 2 : XRD patterns of powder NdN 5 after different heat treatments.

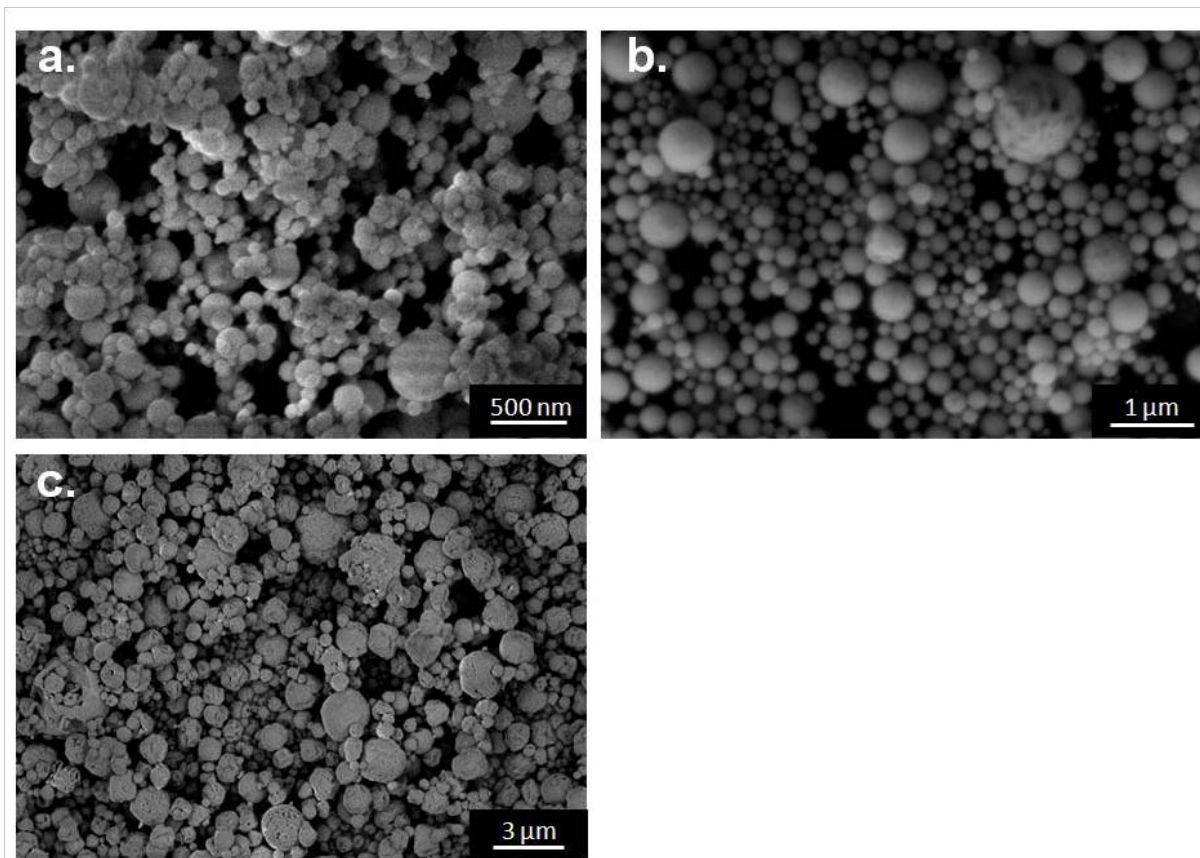


Figure 3: HR-SEM pictures of samples synthesized from nitrates solutions with various concentrations: a. NdN 2 ($C= 5.10^{-4}$ M), b. NdN 5 ($C=5.10^{-3}$ M) and c. NdN 7 ($C= 5.10^{-2}$ M).

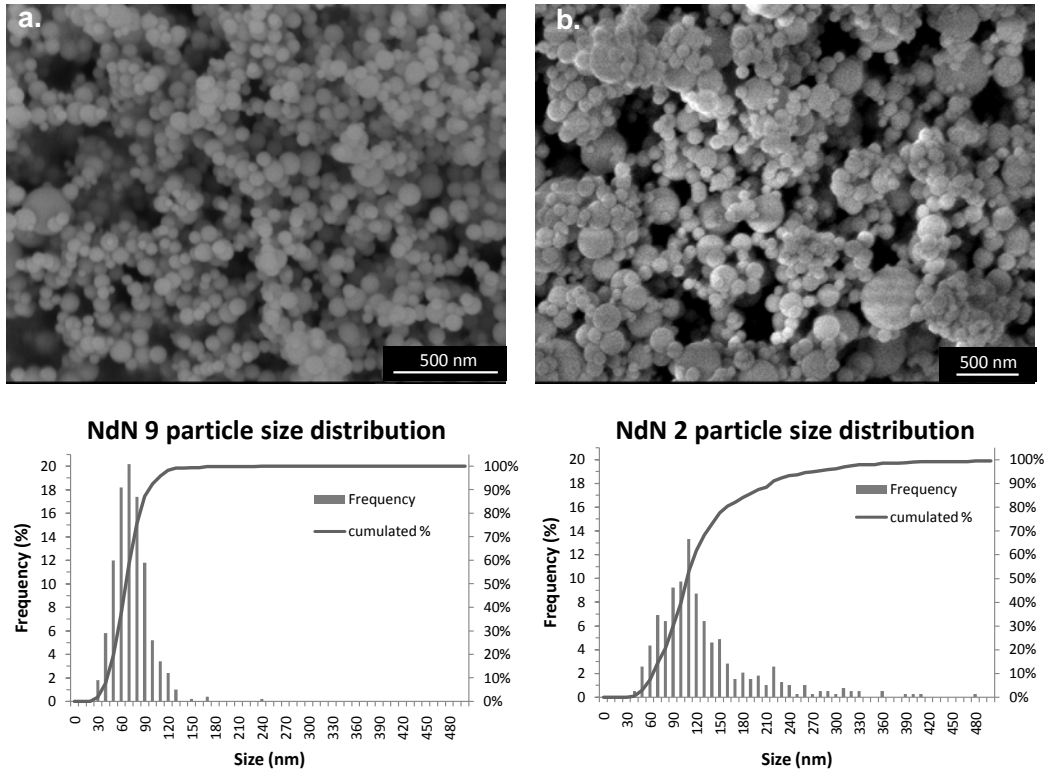


Figure 4: HR-SEM pictures and corresponding particle size distribution of samples a. NdN 9 ($f=2.5$ MHz) and b. NdN 2 ($f=1.7$ MHz).

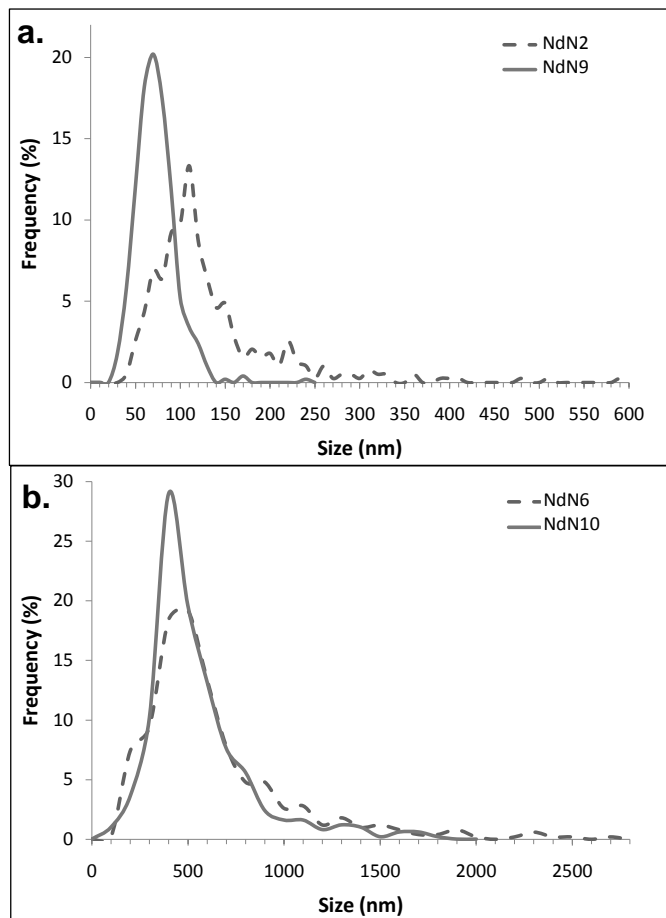


Figure 5: Particle size distribution of samples a. NdN 2 and NdN 9 (5.10^{-4} M) and b. NdN 6 and NdN 10 (5.10^{-2} M). Plain line $f=2.5$ MHz, dash line $f=1.7$ MHz.

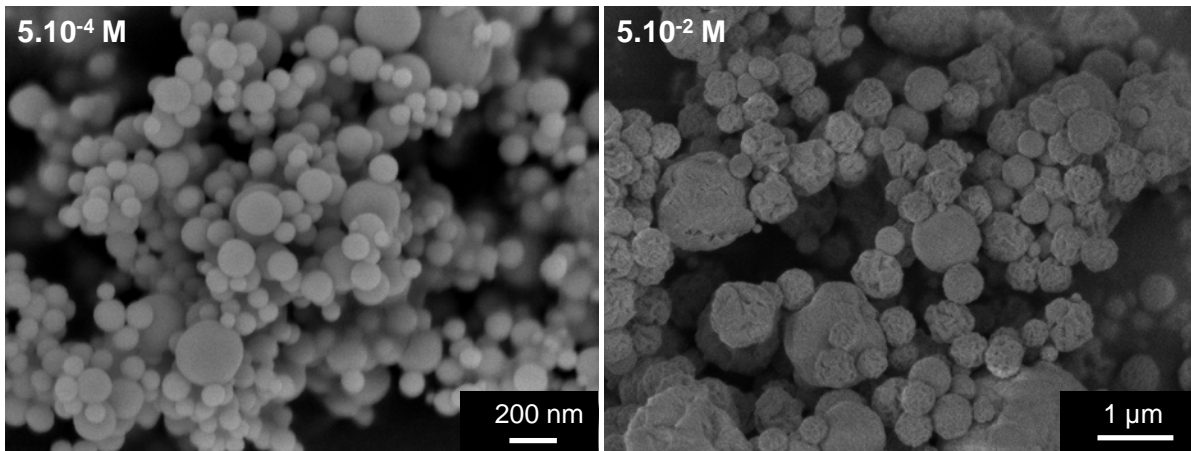


Figure 6: HR-SEM pictures of samples NdN 9 (left) and NdN 11 (right).

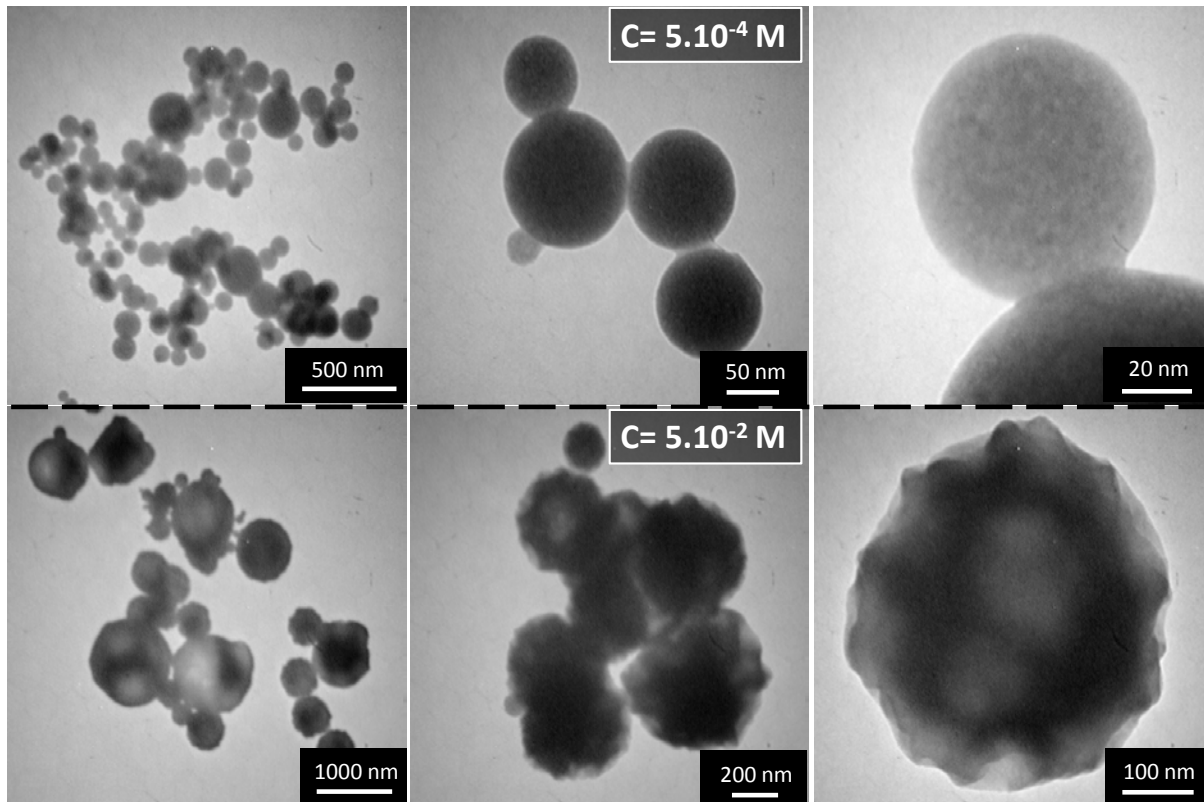


Figure 7: TEM pictures of samples NdN 9 (up) et NdN 11 (bottom).

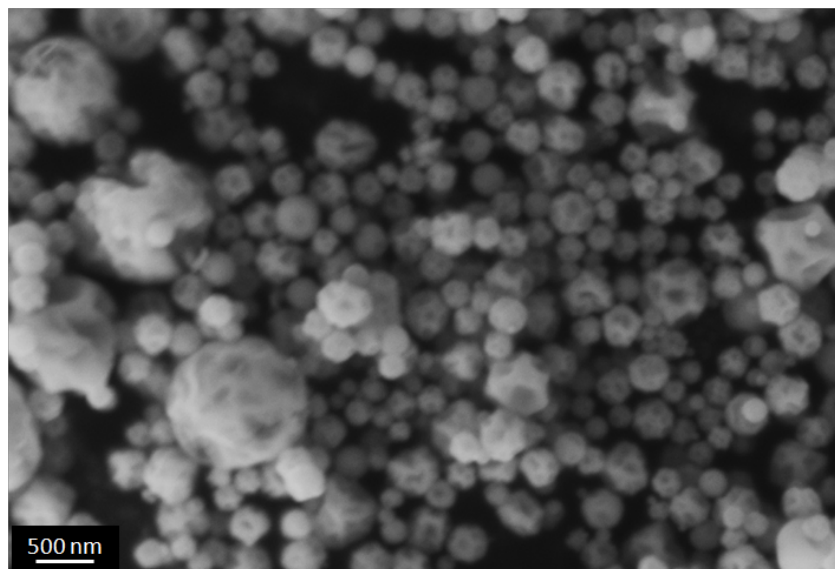


Figure 8: SEM picture of sample NdN 15 synthesized from acetate precursors.

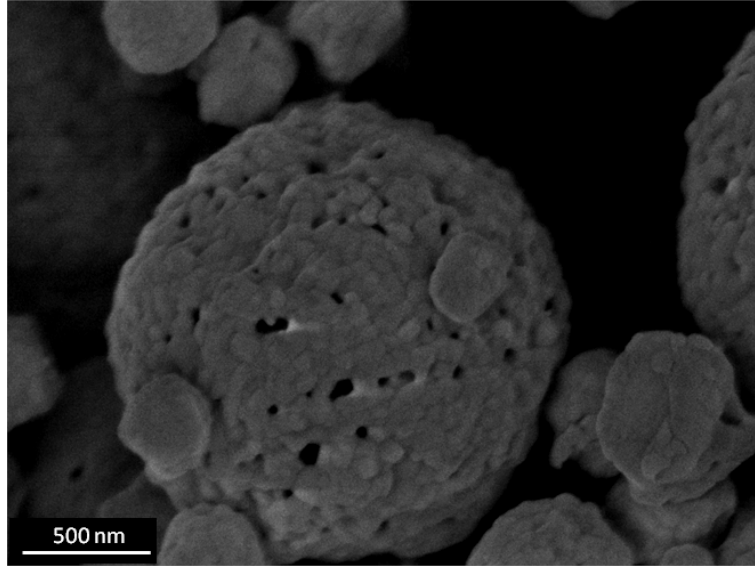


Figure 9: SEM picture of a porous particle in sample NdN 6.